SUPPLEMENTARY INFORMATION

Understanding the molecular basis for the controlled design of ruthenium nanoparticles in microporous aluminophosphates

M. E. Potter,[a,b] J. M. Purkis,[a] M. Perdjon,[c,d] P. P. Wells[c,d] and R. Raja[a]*

a) University of Southampton, Department of Chemistry, Southampton, Hants, SO17 1BJ, UK
b) Georgia Institute of Technology, Department of Chemical and Biochemical Engineering, Atlanta, GA, 30318, USA
c) The UK Catalysis Hub, Research Complex at Harwell, Harwell, Oxon, OX11 0FA, UK
d) Kathleen Lonsdale Building, Department of Chemistry, University College London, Gordon Street, London, WC1H 0AJ, UK

CONTENTS

AlPO substitution mechanisms

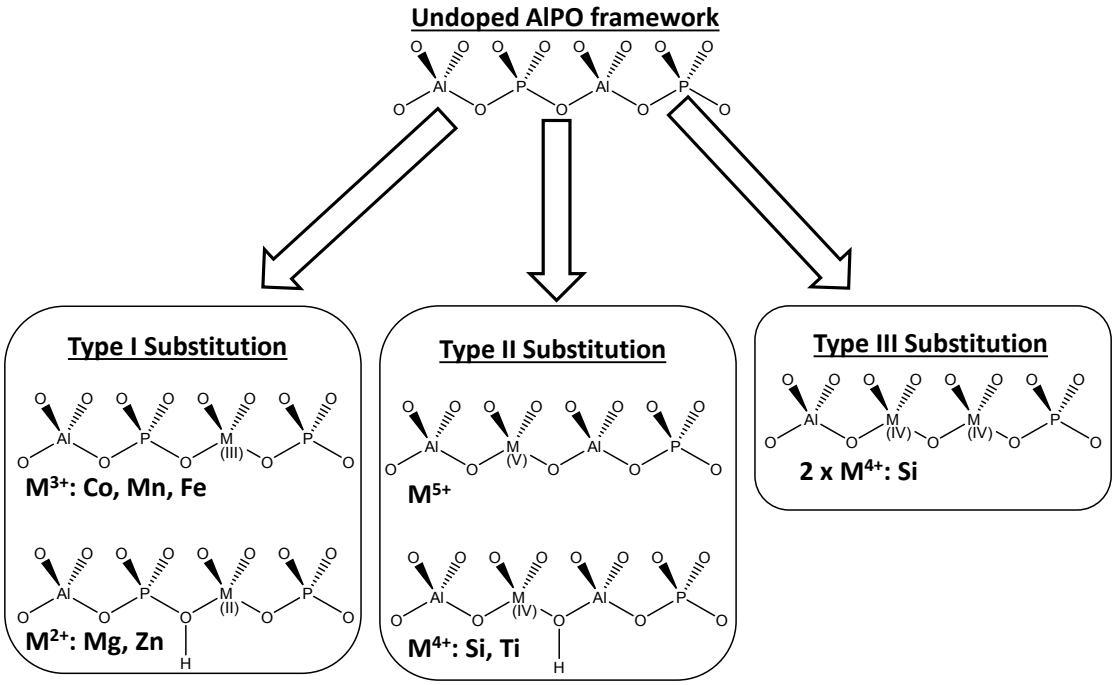

Scheme S1: Detailing the isomorphous metal-substitution mechanisms available in AlPO materials. The Al(III) and P(V) T-atom tetrahedral in the AlPO framework can be replaced with a range of transition-metals, creating isolated active sites.

In-depth structural and textural characterisation

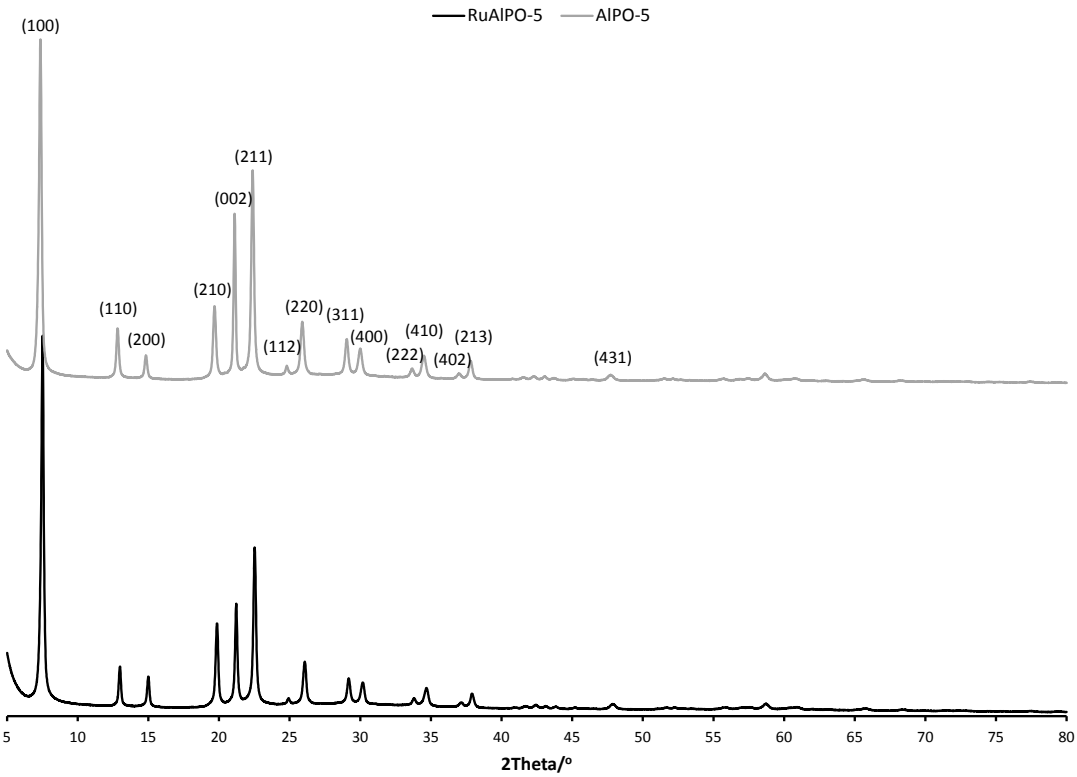

Figure S1: Powder XRD patterns of the AlPO-5 and undoped RuAlPO-5 systems, both showing phase pure AFI.

Table S1: ICP, textural and unit-cell parameters for ruthenium-doped AlPO-5 (RuAlPO-5) and undoped AlPO-5.

	Metal Analysis			BET SSA/m^2g^{-1}	P6cc unit cell parameters	
	Al/wt%	P/wt%	Ru/wt%		a/Å	c/Å
RuAlPO-5-O-400	16.5	20.7	2.90	282	13.70	8.40
AlPO-5	16.7	18.1	-	295	13.69	8.43

Complementary EXAFS and Mass spectrometry data

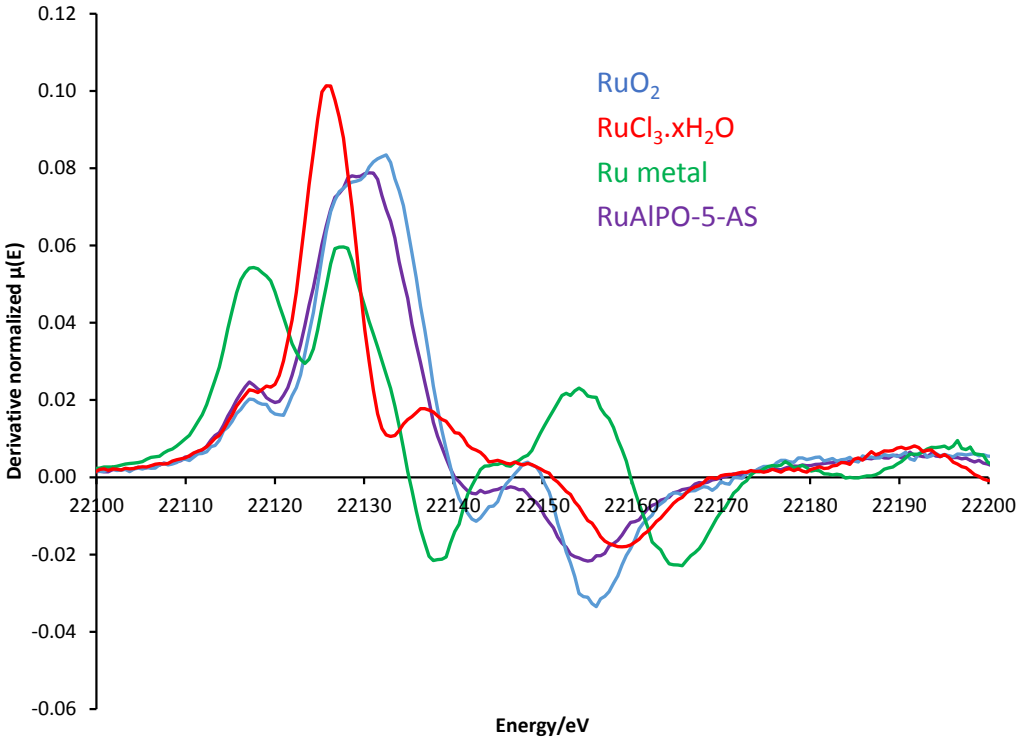

Figure S2: The derivative of μ(E) for standard compounds and RuAlPO-5-AS, confirming the intermediary characteristics of RuAlPO-5-AS between Ru(IV)O_2 and Ru(III)$Cl_3.xH_2O$.

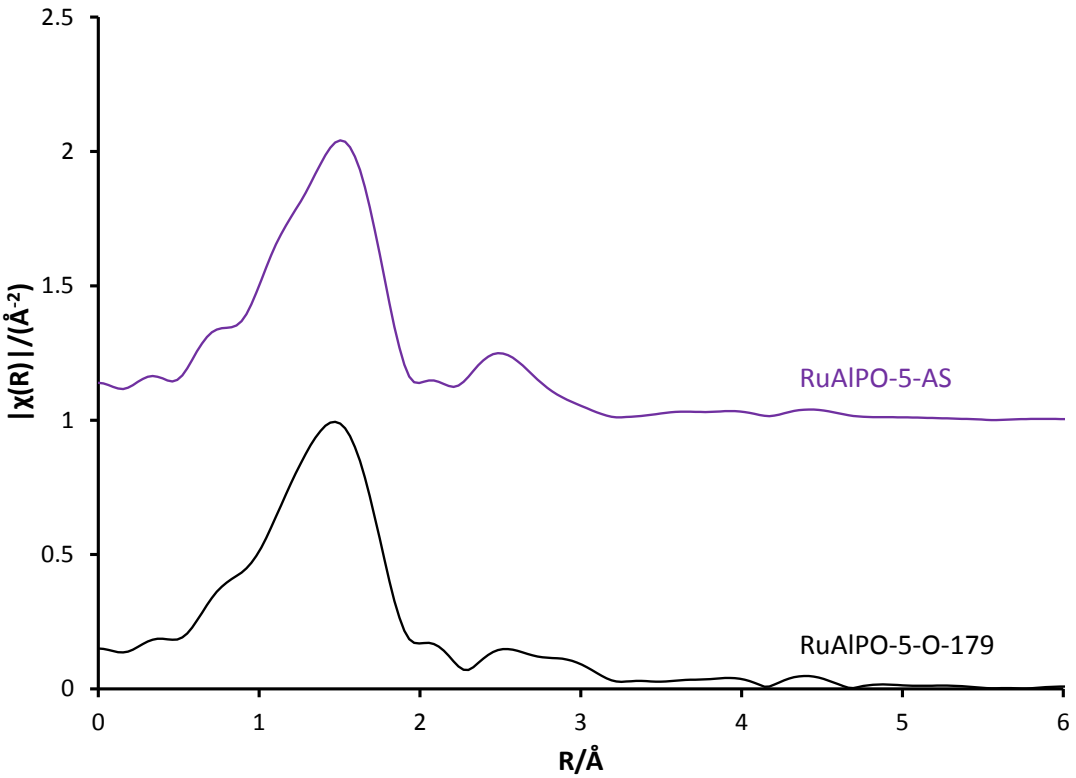

Figure S3: The variations in the magnitude of the k^2 weighted Fourier transform, contrasting the as-synthesised material with one heated to 179 °C under oxidative conditions.

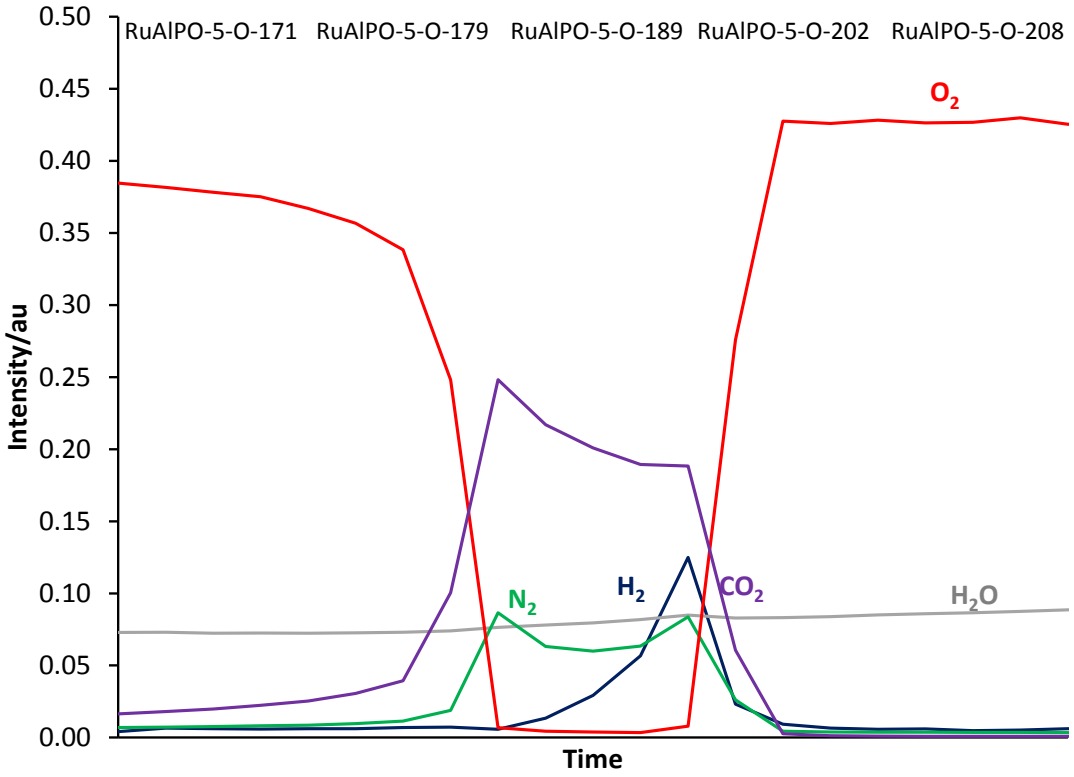

Figure S4: Mass-spec data detailing the evolution of gases between specific scans in the RuAlPO-5-O series, showing the evolution of hydrogen gas.

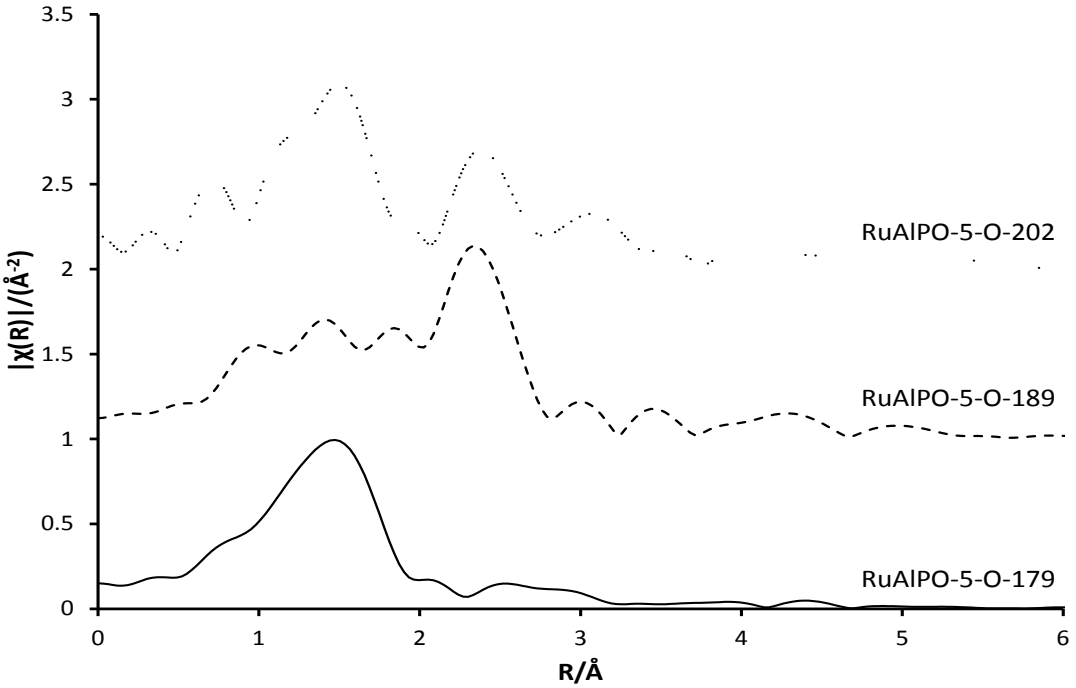

Figure S5: The variations in the magnitude of the k^2 weighted Fourier transform, examining the effect of oxidative calcination on ruthenium with temperature, focussing on the metallic-phase transformations (189 ^{o}C).

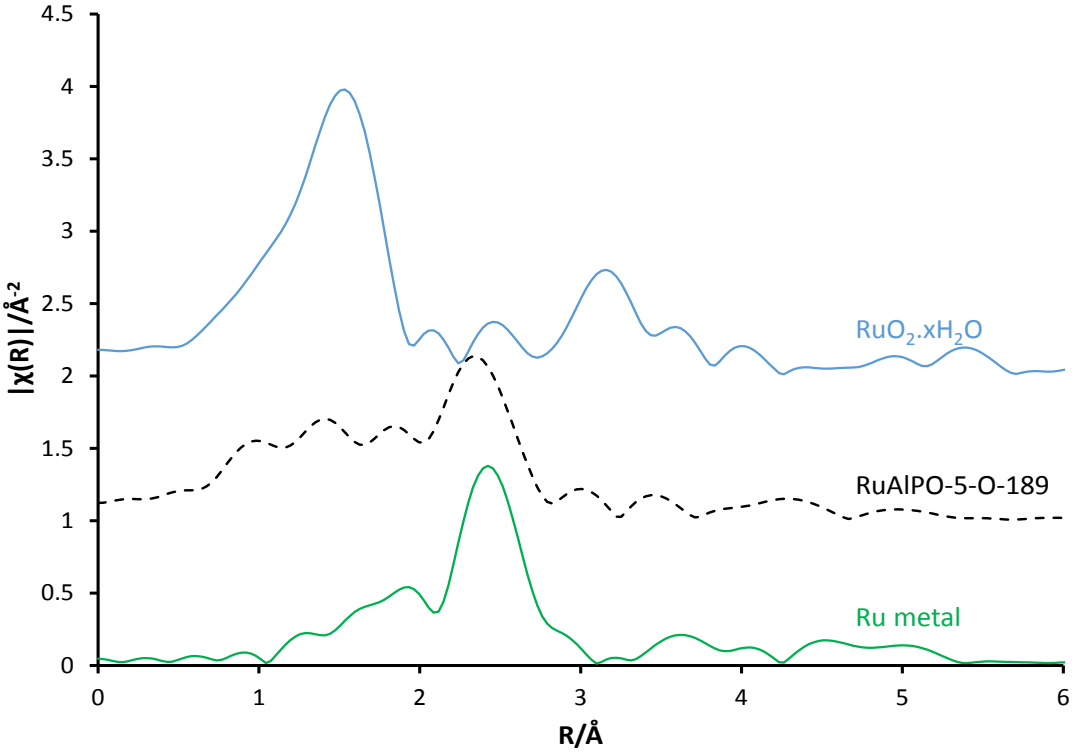

Figure S6: Variations in the magnitude of the k^2 weighted Fourier transform,, examining the effect of oxidative calcination on ruthenium with temperature, focussing on the metallic-phase transformations (189 ^{o}C), contrasting with known standards.

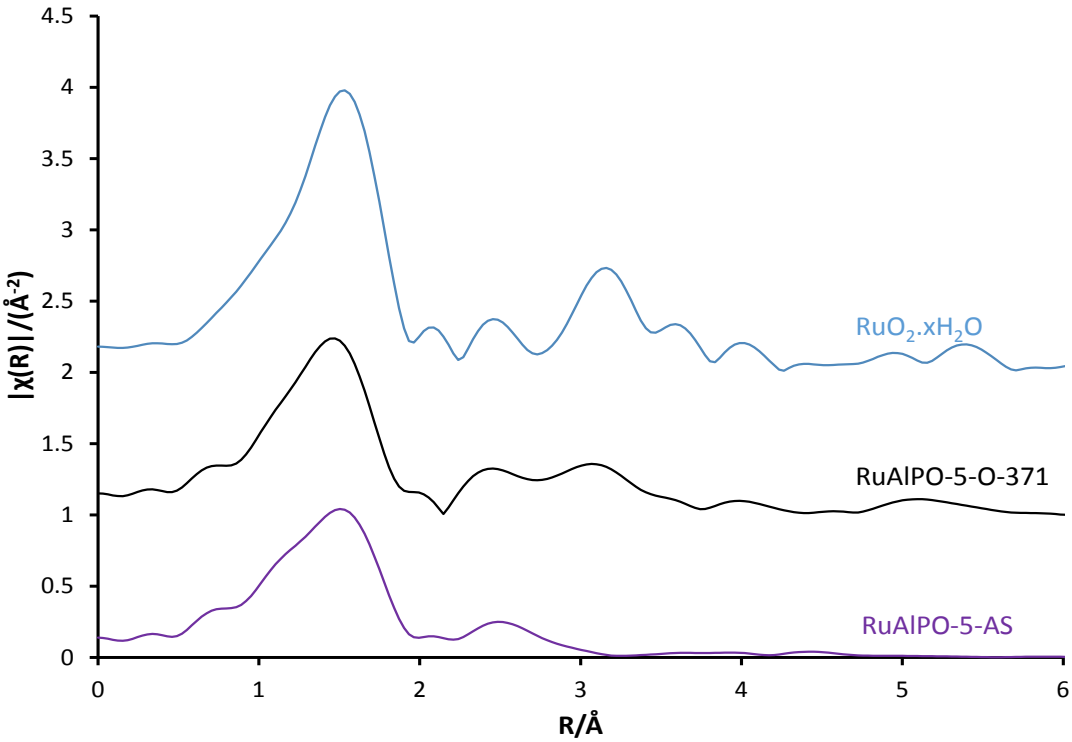

Figure S7: Changes in the magnitude of the k^2 weighted Fourier transform, probing the effect of oxidative annealing on ruthenium with temperature and contrasting the as-synthesised oxidic environment with that obtained under more extreme annealing conditions.

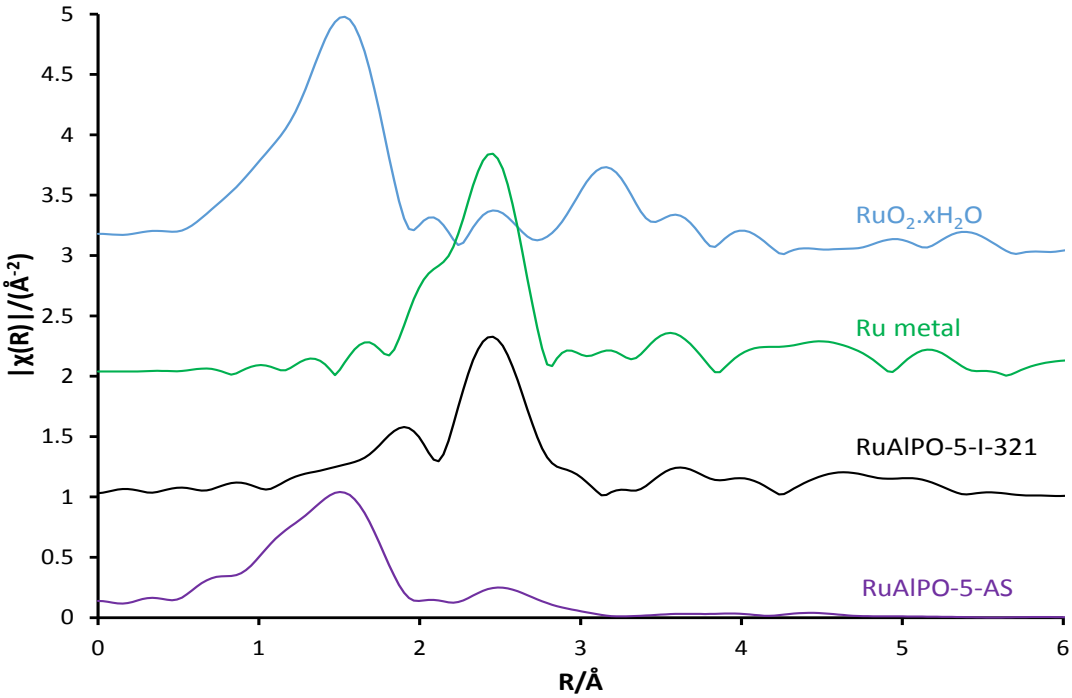

Figure S8: Variations in the magnitude of the k^2 weighted Fourier transform, examining the effect of inert annealing on ruthenium with temperature and contrasting the as-synthesised oxidic environment with that obtained under more extreme annealing conditions.

TEM and EDS images

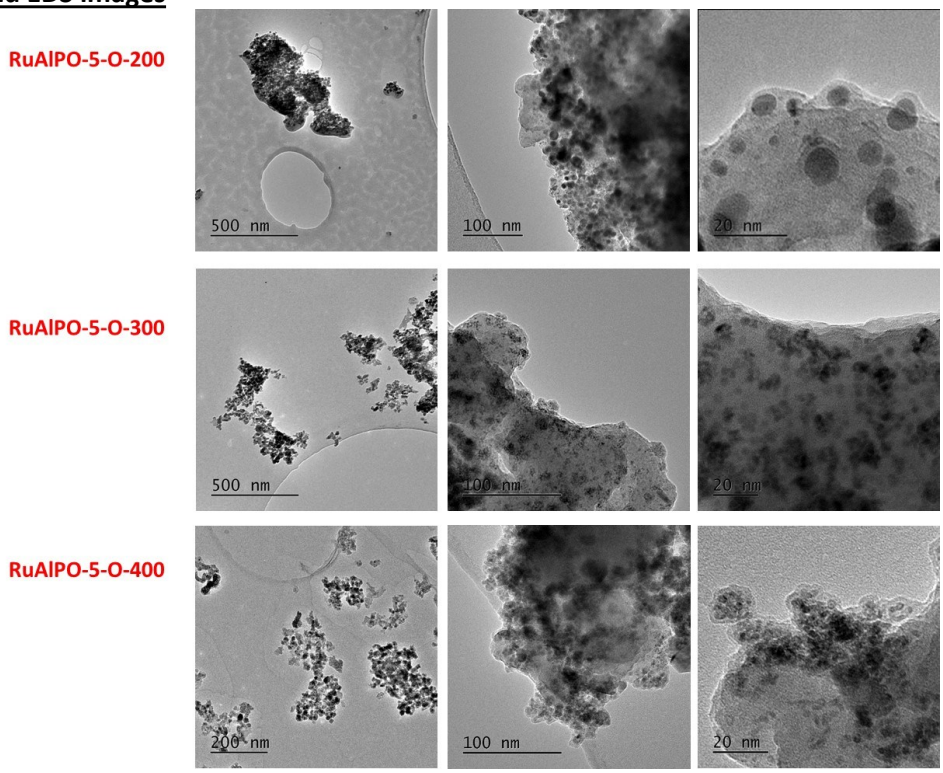

Figure S9: TEM images of the RuAlPO-5-O series at increasing temperature showing small nanoparticles (< 3 nm) in all cases. Increases in temperature lead to significant nanoparticle agglomeration.

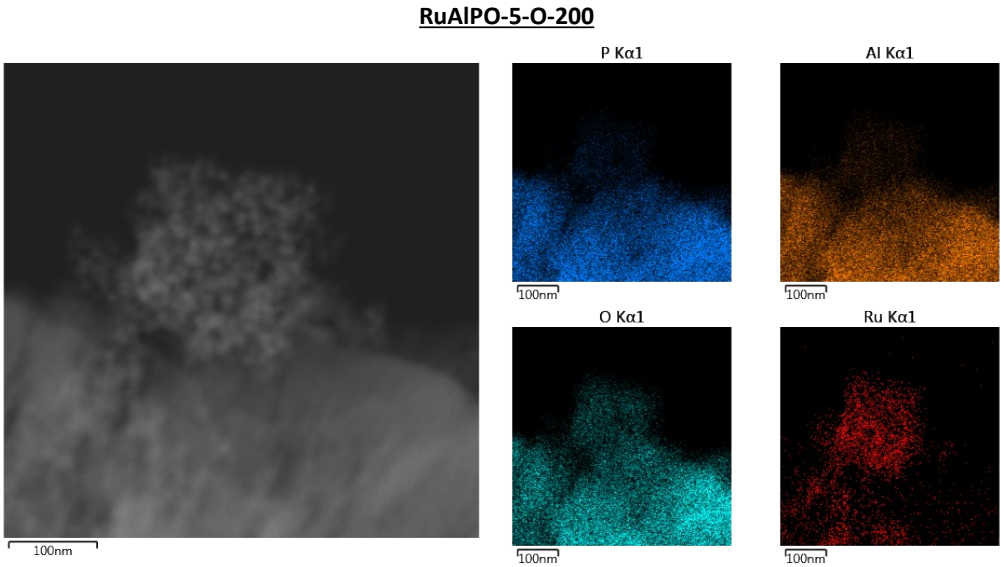

Figure S10: Energy dispersive X-ray spectroscopy images highlighting the elemental distribution of RuAlPO-5-O-200. The figures show ruthenium is present in areas where the oxygen, aluminium and phosphorus signals are weakest suggesting metallic ruthenium.

RuAlPO-5-O-300

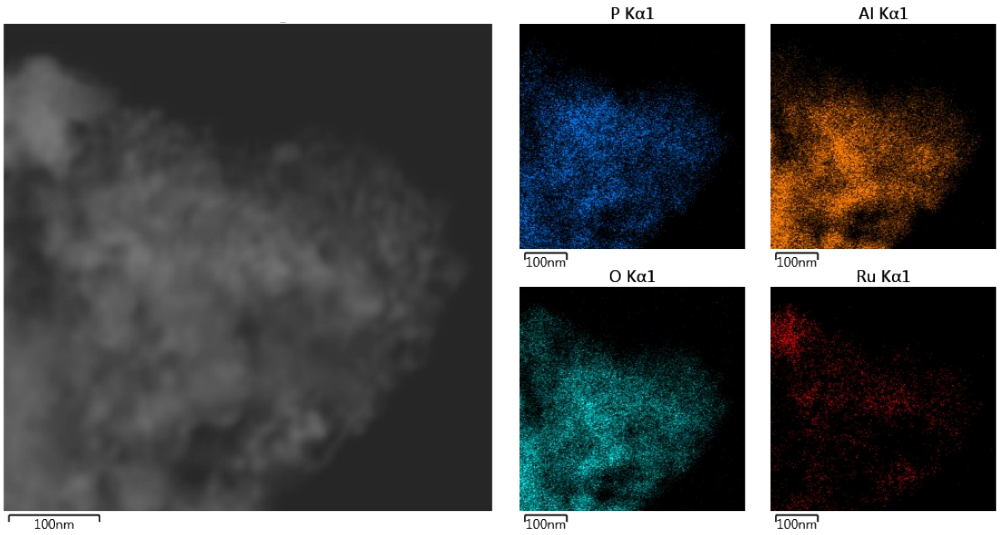

Figure S11: Energy dispersive X-ray spectroscopy images highlighting the elemental distribution of RuAlPO-5-O-300. The figures show ruthenium is present in areas where the oxygen, aluminium and phosphorus signals are weaker suggesting metallic ruthenium with some oxidic content.

RuAlPO-5-O-400

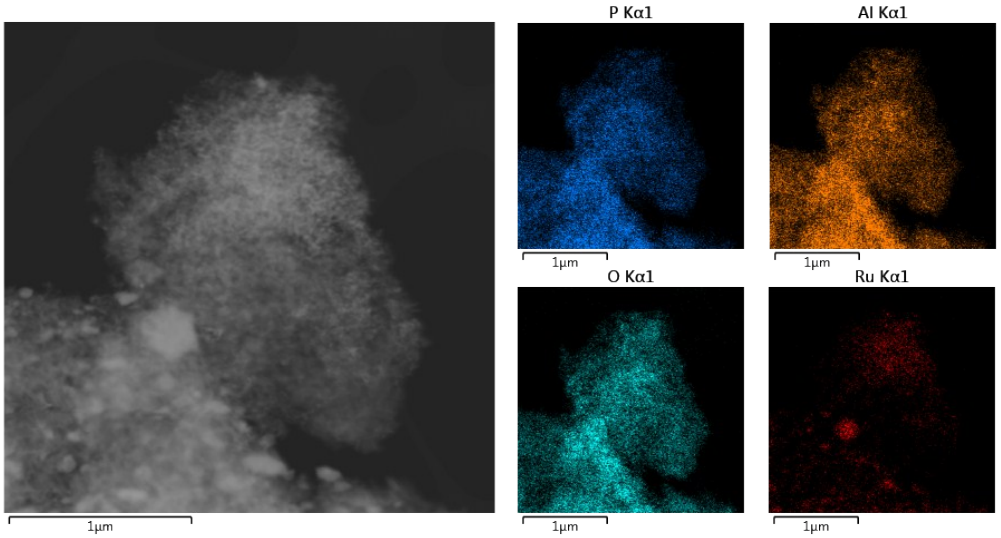

Figure S12: Energy dispersive X-ray spectroscopy images highlighting the elemental distribution of RuAlPO-5-O-400. The figures show oxygen intensity is invariant of ruthenium distribution, suggesting ruthenium oxide has been formed.

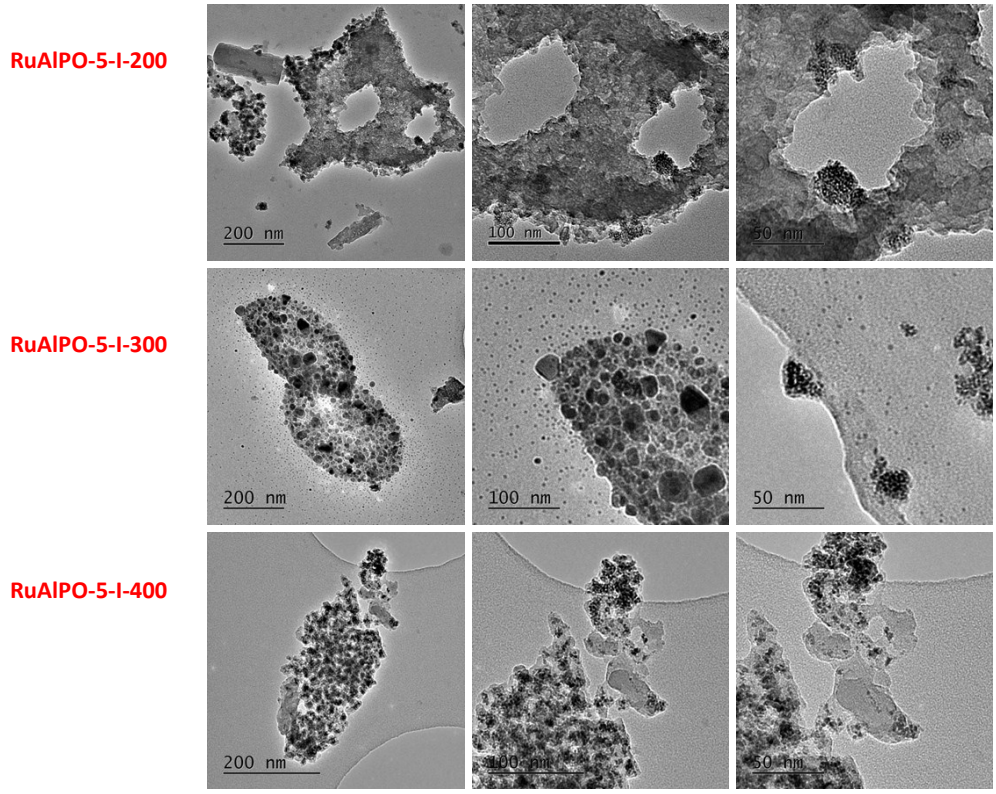

Figure S13: TEM images of the RuAlPO-5-I series at increasing temperature showing small nanoparticles (< 3 nm) in all cases. Increases in temperature lead to significant nanoparticle agglomeration.

Further catalytic data

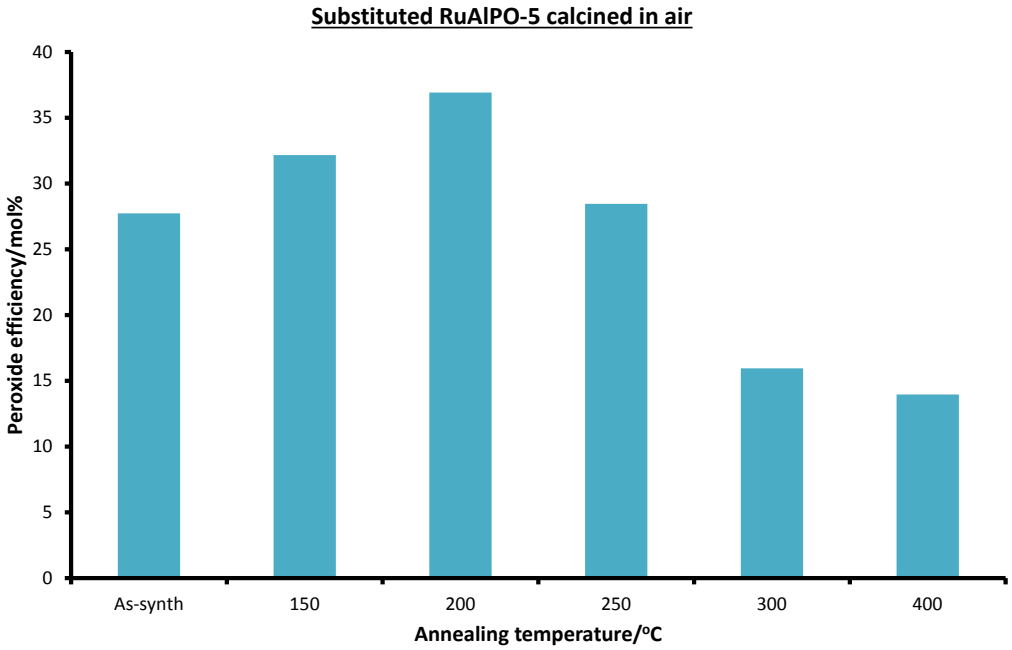

Figure S14: Comparing the effect of annealing temperature under air atmosphere on the peroxide efficiency of RuAlPO-5 for the oxidation of cyclohexane. Conditions: 13 mmol cyclohexane, 13 mmol TBHP (70 wt% in H_2O), 0.05 g of RuAlPO-5 and 5 ml of acetone, 70 °C, 6 hours.

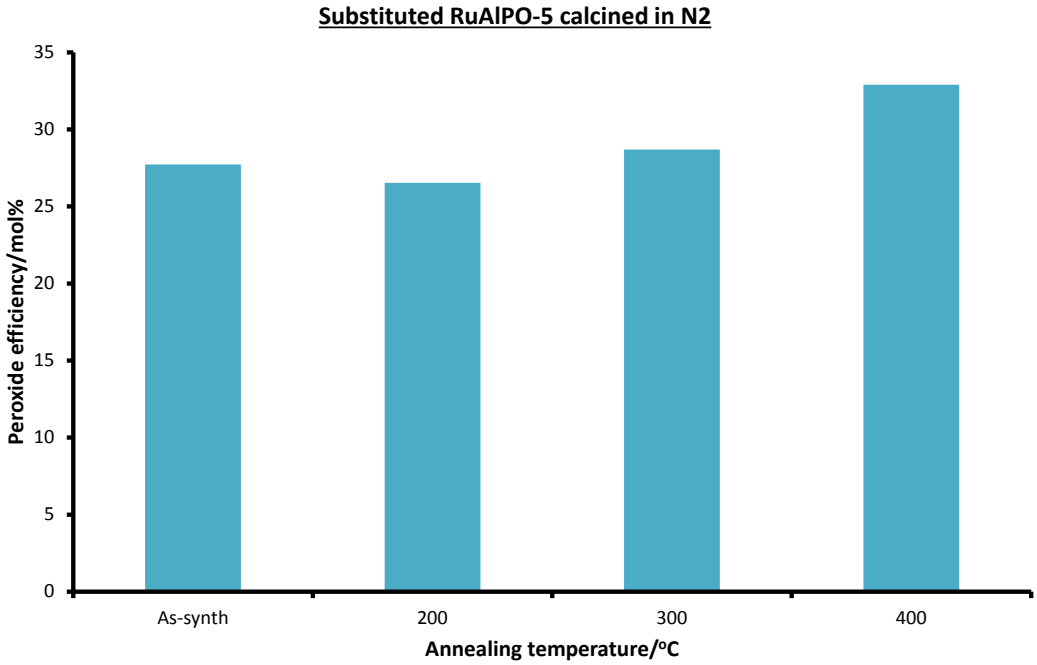

Figure S15: Comparing the effect of annealing temperature under nitrogen atmosphere on the peroxide efficiency of RuAlPO-5 for the oxidation of cyclohexane. Conditions: 13 mmol cyclohexane, 13 mmol TBHP (70 wt% in H_2O), 0.05 g of RuAlPO-5 and 5 ml of acetone, 70 °C, 6 hours.

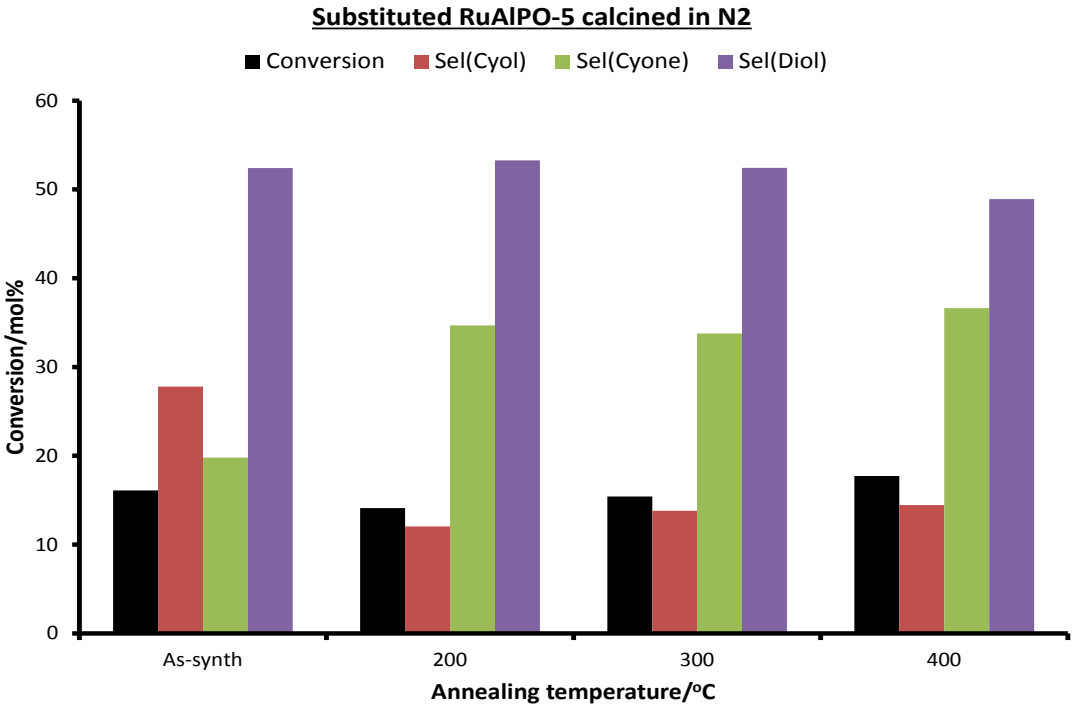

Figure S16: Comparing the effect of annealing temperature under nitrogen atmosphere on the conversion and selectivity profiles of RuAlPO-5 for the oxidation of cyclohexane. Conditions: 13 mmol cyclohexane, 13 mmol TBHP (70 wt% in H_2O), 0.05 g of RuAlPO-5 and 5 ml of acetone, 70 °C, 6 hours.

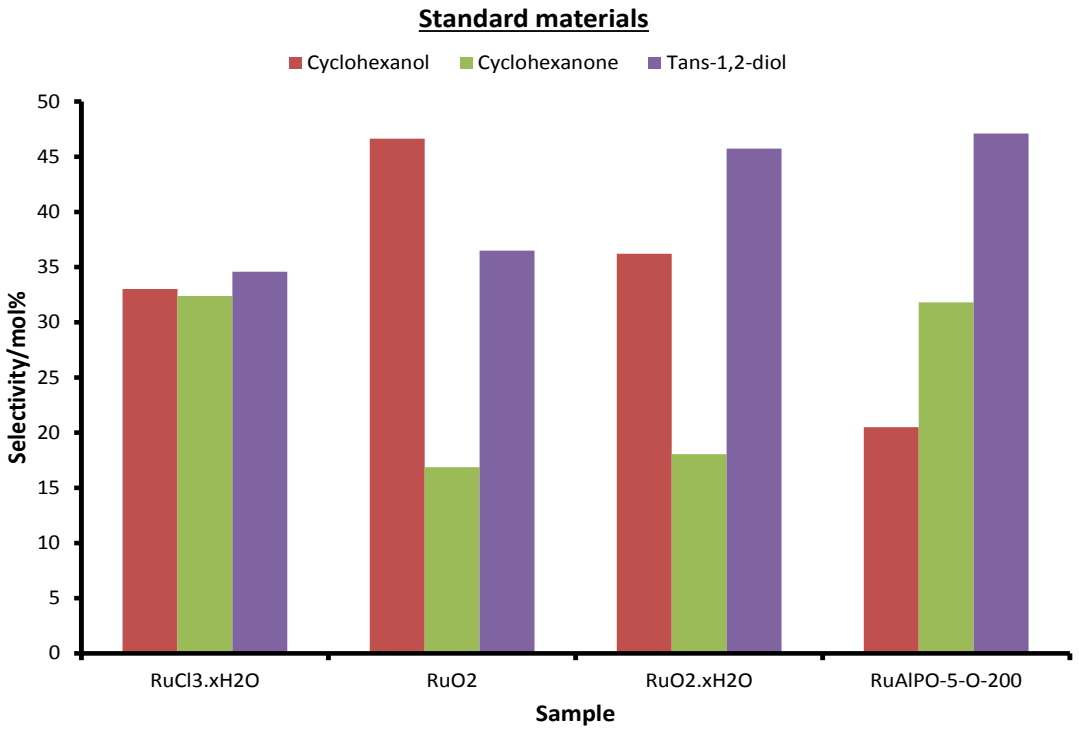

Figure S17: Comparing the selectivity of different ruthenium containing systems for the oxidation of cyclohexane. Conditions: 13 mmol cyclohexane, 13 mmol TBHP (70 wt% in H_2O), 0.05 g of RuAlPO-5 and 5 ml of acetone, 70 ^oC, 6 hours.

Repeatability

Table S2: Detailing reproducibility between experiments and different batches of catalysts. All units are in mol%.

Sample	Conversion	Yield(Cyol)	Yield(Cyone)	Yield(Diol)
RuAlPO-5-I-400	17.7	2.6	6.5	8.7
RuAlPO-5-I-400 Repeat Reaction[a]	15.1	4.2	6.2	4.5
RuAlPO-5-O-200	20.7	4.2	6.6	9.9
RuAlPO-5-O-200 Separate Batch[b]	18.1	5.1	4.1	9.0

Conditions: 13 mmol cyclohexane, 13 mmol TBHP (70 wt% in H_2O), 0.05 g of RuAlPO-5 and 5 ml of acetone, 70 ^oC, 6 hours.

a) This reaction was performed with the same batch of catalyst that the characterisation and catalysis was performed on. The error in conversion is within 3%, the threshold for GC analysis.
b) This reaction was performed on a separate batch of catalyst to show the reproducibility of this method. Note errors are all within 2.6 mol%, lower than that of the threshold for GC error.